SPACE Conferences and Exposition
13 - 16 September 2016, Long Beach, California
AIAA SPACE 2016

Aerothermal Design of the Hexafly-INT Glider

Roberto Scigliano[1], Giuseppe Pezzella[2], Marco Marini[3], Sara Di Benedetto[4]
[1]*CIRA, Italian Aerospace Research Center, Via Maiorise, 81043 Capua (CE), Italy*

and

Johan Steelant[5]
[2]*ESA-ESTEC, European Space Agency, Keplerlaan 1, 2200 AZ Noordwijk, The Netherlands,*

Over the last years, innovative concepts of civil high-speed transportation vehicles were proposed. These vehicles have a strong potential to increase the cruise range efficiency at high Mach numbers, thanks to efficient propulsion units combined with high-lifting vehicle concepts. In this framework the Hexafly-INT project has the scope to test in free-flight conditions an innovative gliding vehicle with several breakthrough technologies on-board. This work describes the aero-thermal design processes of the Hexafly-INT Experimental Flight Test Vehicle, namely EFTV.

Nomenclature

Y^+	=	non-dimensional wall distance
M_∞	=	free-stream Mach number
ε	=	surface emissivity
Re_∞	=	free-stream Reynolds number
Λ	=	wing sweep angle
H_0	=	total enthalpy
EFTV	=	Experimental Flight Test Vehicle
FE	=	Finite Element

I. Introduction

Over the last years, innovative concepts of civil high-speed transportation vehicles were proposed. These vehicles have a strong potential to increase the cruise range efficiency at hypersonic Mach numbers, thanks to efficient propulsion units combined with high-lifting vehicle concepts. Nonetheless, performing flight tests will be the only and ultimate proof to demonstrate the technical feasibility of these new promising concepts and would result into a major breakthrough in high-speed flight. In this framework the Hexafly-INT project, funded by European Commission by means of 7th Framework Programme, intends to test in free-flight conditions an innovative gliding vehicle with several breakthrough technologies on-board. This approach will create the basis to gradually increase the readiness level of a consistent number of technologies suitable for hypervelocity flying systems. The vehicle design, manufacturing, assembly and verification will be the main driver and challenge in this project, in combination with a mission tuned sounding rocket. The prime objectives of this free-flying high-speed cruise vehicle aim at:

- a conceptual design demonstrating a high aerodynamic efficiency in combination with high internal volume;
- controlled level flight at a cruise Mach number of 7 to 8;

[1] Research Engineer, Thermal Structures and Thermal Control Technologies and Design, r.scigliano@cira.it.
[2] Research Engineer, Aerothermodynamics, Analysis and extrapolation to Flight Lab, g.pezzella@cira.it
[3] Research Engineer, Space Department, Technology Integration, m.marini@cira.it
[4] Research Engineer, Aeronautics - System Engineering, s.dibenedetto@cira.it
[5] Research Engineer, Propulsion Design and Aerothermodynamics Section (TEC-MPA), Johan.Steelant@esa.int

- an optimal use of advanced high-temperature materials and/or structures;
- an evaluation of the sonic boom impact by deploying dedicated ground measurement equipment.

The aerodynamic performance from Mach 7 down to Mach 2 can be determined as a secondary objective. In this framework, the present research effort describes the aero-thermal design process of the Hexafly-INT Experimental Flight Test Vehicle, namely EFTV.

The glider aeroshape design makes maximum use of databases, expertise, technologies and materials elaborated in previously European community co-funded projects ATLLAS I & II, LAPCAT I & II, and HEXAFLY. [1,2,3,9]

The paper will present results for both CFD and Finite Element thermal analysis, performed in the most critical phases of the experimental flight.

These analyses lead to a proper material selection[4,5,6]. Different classes of materials have been preliminarily selected and analysed for the EFTV structure, namely: titanium alloy, copper, C/C-SiC and zirconia for surface coatings. Titanium alloys exhibit a unique combination of mechanical and physical properties and corrosion resistance which have made them desirable for critical, demanding aerospace applications, also in high temperatures conditions. Copper is employed as a heat sink to accommodate the thermal energy in some critical components such as the nosetip. C/C-SiC developed at DLR and tested in different high temperatures applications (e.g. HIFiRE and SHEFEX) is considered for ailerons and for the wing leading edges. A zirconia coating layer has been also considered to protect titanium and copper components, increasing the surface emissivity and confining the larger temperatures on the layer itself.

Thermal and mechanical properties of titanium alloy and zirconia coating have been provided by TsAGI, Tsentralniy Aerogidrodinamicheskiy Institut (Central Aerohydrodynamic Institute), which is in charge of the EFTV manufacturing. The aero-thermal environment, taken into account, is that one during the test window at cruise Mach numbers, in particular regarding aerothermodynamic loads acting on the vehicle along the flight path.

II. Flight Trajectory

The preliminary mission trajectory was generated by DLR-Moraba for what concerns the VS43 launch vehicle, assuming a total payload mass of 800kg (EFTV, ESM, launch vehicle service module, fairing), and by Gas Dynamics Ltd. (GDL) for both the descending "train" EFTV+ESM and the EFTV alone after the separation from ESM, assumed at 50km of altitude, up to 20km of altitude. An inviscid Aerodynamic Database (AEDB) was generated by DLR Braunschweig. The hypothesis of continuum regime was also verified for the last two phases of flight trajectory.

GDL generated a number of 3 degree-of-freedom (DoF) planar trajectories for the hypersonic glider considering turbulent viscous effects (conservative approach), and with a limited level of optimization. In particular, the viscous correction was added to the axial force coefficient C_A (during the trimmed aerodynamics/trajectory calculation) by means of an engineering estimation of viscous forces acting on the vehicle, considered as a flat plate with a total wetted area of 7.35m^2. The skin-friction coefficient was evaluated for a compressible turbulent boundary layer using the reference temperature method (Schoenherr correlation), i.e.

$$C_f = 0.455 \frac{\rho_r}{\rho_e} \log_{10}\left(\frac{\rho_r u_e L}{\mu_r}\right)^{-2.58} \quad (1)$$

In Eq. (1) *r* stands for conditions evaluated at the turbulent reference temperature, *e* for free-stream conditions.

After an analysis of the train trajectory, from 60km to 50km, whose inviscid aerodatabase was provided by CIRA (the aerodynamic characterization of EFTV+ESM was performed only at M=8, according to the train flight profile provided by DLR-Moraba), the separation of EFTV from ESM was assumed at 50km altitude since typical control authority criteria are satisfied for a dynamic pressure higher than 3000 Pa (see Figure 1, left). In particular, separation was calculated to occur at the following conditions: 49.94 km altitude, Mach=7.07, AoA=6.83 deg, Flight Path Angle (FPA) =-20.53 deg, in a condition of natural trim for the descending "train" for zero sideslip (see Figure 1, right).

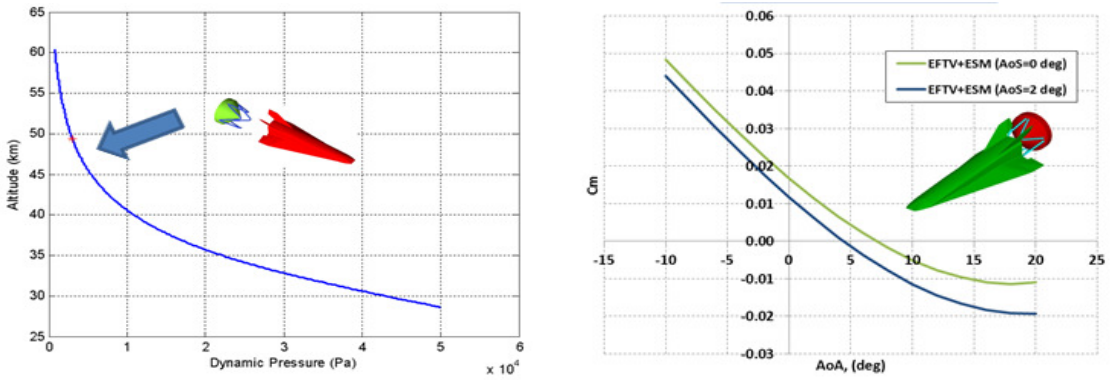

Figure 1. EFTV-ESM separation point (left) and "train" total pitching moment (right).

For the glider trajectory calculation, GDL assumed an EFTV mass of 350kg and its centre of gravity coinciding with the MRC (1.455, 0.0, 0.12) [m], i.e. at 57% of the glider full length. EFTV's AoA initial schedule was based on a profile defined by CIRA that satisfies control authority criteria.

Trajectory B-viscous was finally selected as reference having the longest duration and the highest mission parameters for the Phase I (experimental window), i.e. L/D $\geq$ 4 with Mach number $\geq$ 7. Even though less performant for the Phase II of the flight, trajectory B-viscous was considered as the lower reference trajectory of the flight corridor as it has a built-in margin during future trajectory consolidation, and it is adopted as reference for the thermo-structural analysis. Any future optimized trajectory will not need questioning whether the EFTV will be not affected along it w.r.t. structural and thermal loads.

Figure 2 to Figure 4 show the main parameters of trajectory B-viscous, in particular highlighting the sequence of the critical (and sizing) events:

1) ESM/EFTV separation,
2) maximum Mach number (M=7.5),
3) maximum stagnation-point heat flux (computed by an engineering formula),
4) possible laminar-to-turbulence transition,
5) maximum angle of attack, maximum a/g, largest (negative) aileron deflection,
6) pull-out manoeuvre,
7) maximum L/D,
8) maximum dynamic pressure (and Reynolds number),
9) horizontal hypersonic flight/gliding flight, and 10) end of mission at about M=2.

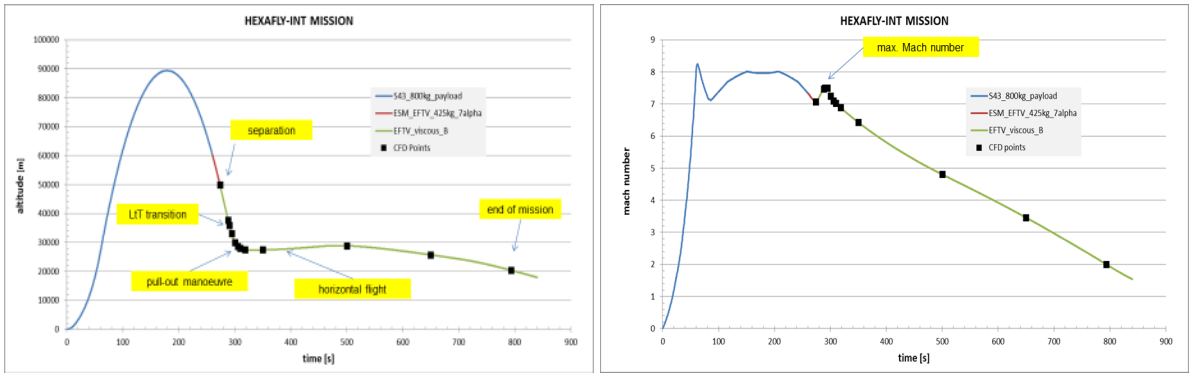

Figure 2. Altitude (left) and Mach number (right) time histories.

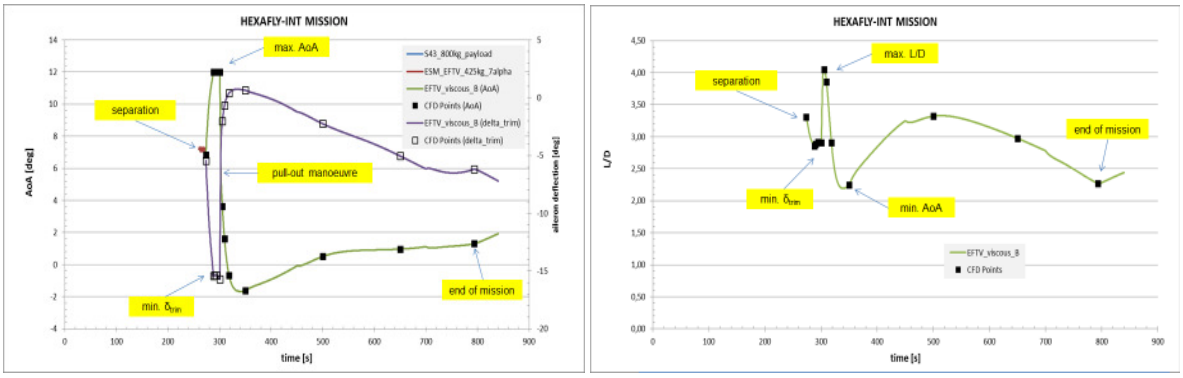

Figure 3. Angle-of-attack and aileron deflection (left) and aerodynamic efficiency (right) time histories.

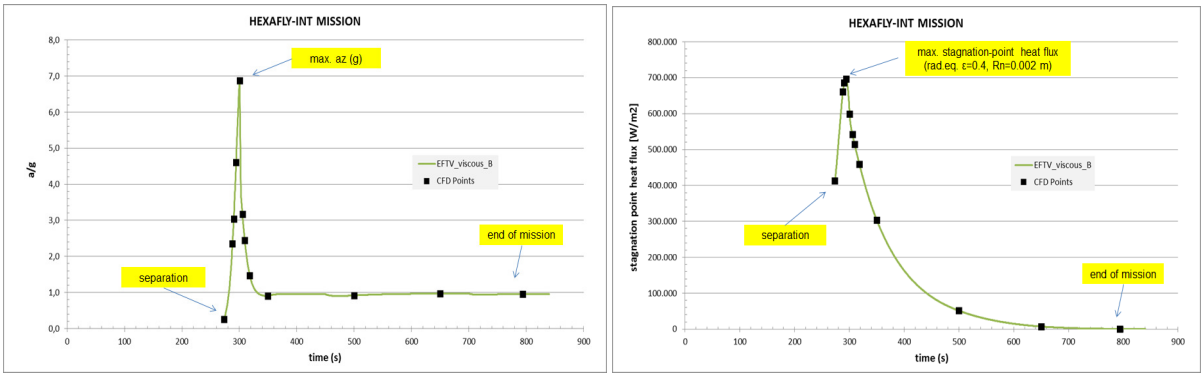

Figure 4. G-load (left) and nosetip stagnation-point heat flux (right) time histories.

The black full squares displayed from Figure 2 to Figure 4 represent the flight conditions selected for the EFTV aerodynamic and aerothermodynamic characterization by means of viscous CFD simulations, according to a "Trajectory-Based" design approach. The test matrix is reported in Table 1 and has been selected with three main objectives: i) to verify the trim conditions along the reference trajectory extracted by inviscid AEDB generated by DLR (and corrected by GDL for viscous effects); ii) to provide mechanical and thermal loads as inputs for thermo-structural analysis of whole EFTV configuration (CIRA) and some components such as wing leading edge and aileron (DLR-Stuttgart) and vertical fin (University of Sidney); and iii) to provide surface distribution of pressure, heat flux and temperature for the in-flight measurement system design and layout optimization (DRL-Cologne).

	RUN ID	TIME (S)	H_∞ (M)	T_∞ (K)	M_∞	AOA (DEG)	P_∞ (PA)	δ_ELEV (DEG)	H_0 (MJ/KG)
EFTV/ESM SEPARATION	EFTV-065	273.50	49942.00	270.65	7.07	6.83	80.35	-5.46	2.99
	EFTV-066	288.14	37716.85	244.03	7.46	12.00	392.18	-15.44	2.98
MAXIMUM MACH	EFTV-067	290.39	35947.24	239.14	7.50	12.00	502.25	-15.39	2.94
MAXIMUM HEAT FLUX@NOSETIP	EFTV-068	294.44	33059.99	231.14	7.50	12.00	760.60	-15.38	2.85
MAXIMUM AOA, G-LOAD	EFTV-069	300.52	29936.43	226.45	7.25	12.00	1208.45	-15.72	2.62
MAXIMUM L/D	EFTV-070	305.49	28652.17	225.17	7.10	3.62	1465.01	-2.02	2.51
	EFTV-071	309.55	28040.09	224.57	7.03	1.63	1606.45	-0.68	2.46
MAXIMUM DYN. PRESSURE, RE_L	EFTV-072	318.37	27461.55	223.99	6.88	-0.66	1753.11	0.41	2.36
	EFTV-073	350.00	27444.96	223.98	6.42	-1.63	1757.51	0.64	2.08
	EFTV-074	500.05	28854.96	225.37	4.80	0.51	1421.03	-2.25	1.27
	EFTV-075	649.95	25720.26	222.27	3.46	0.97	2283.67	-5.04	0.76
END OF MISSION	EFTV-076	793.56	20384.69	216.97	2.00	1.31	5206.06	-6.17	0.39

Table 1. CFD Test Matrix.

III. Aerothermodynamic Calculations

The aerothermal environment the vehicle has to withstand during the mission has been addressed in the light of the trajectory-based design approach.[8] According to this approach, aerothermal CFD simulations are performed at a finite number of "critical" points on the given trajectory. With this in mind, the time history of stagnation point heat flux has been sampled in twelve "critical" points, as shown from Figure 2 to Figure 4, such as maxima for dynamic pressure, heat flux, and aerodynamic efficiency *et cetera*.

At each trajectory point viscous simulations are performed and results provided as input of a detailed transient thermal analysis, detailed hereinafter. The CFD test matrix, provided in Table 1, consists of twelve different aileron settings in order to characterize also the flap thermal loads. These Navier-Stokes simulations were carried out by CIRA as part of the more extended viscous EFTV AEDB presently ongoing at ESA, CIRA and TsAGI.

For each simulation in Table 1 a computational grid has been generated by using ICEMCFD® software. To this end, the glider aeroshape has been simplified by removing the antennas and closing the aileron's hingeline gap and fitting, whereas the aileron's lateral gap has been left open. Mesh generation takes advantage of unstructured hybrid grid approach. Therefore, tetrahedrons and prisms discretized the flow and the boundary layer, respectively. An example of grid domain is shown in Figure 5, where the mesh on symmetry plane and vehicle surface is provided. Typically, for the present flight conditions 10 millions of cells have been necessary for half configuration, and in the cases of turbulent boundary layer assumption the condition of $Y^+=O(1)$ at wall also has been verified.

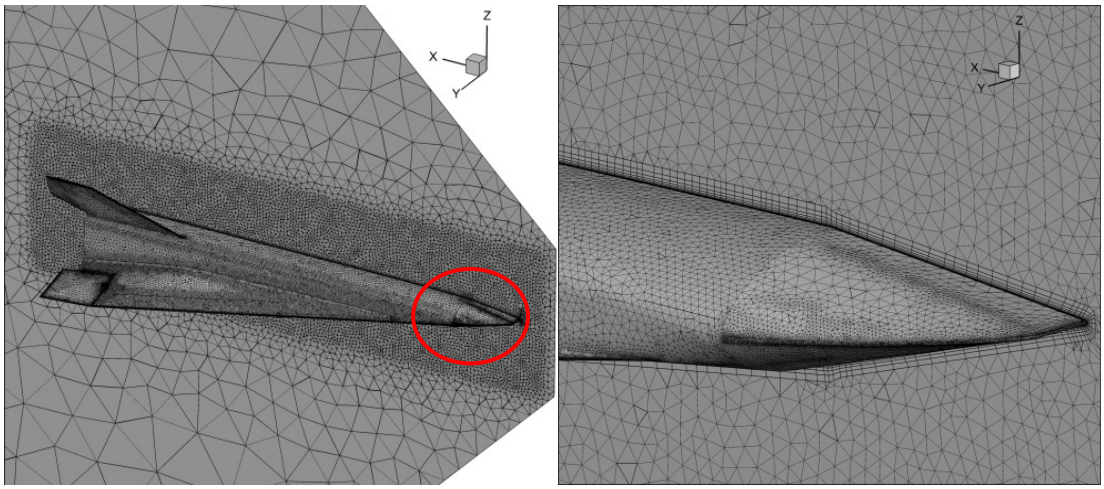

Figure 5. EFTV surface and symmetry plane grid.

The CFD simulations by CIRA have been performed by using the commercial code ANSYS FLUENT® Vs. 14 (parallel version for 12÷16 processors), which solves the Reynolds Averaged Navier-Stokes (RANS) equations on hybrid grids by means of the finite volume approach. FLUENT® uses a Flux Difference Splitting (FDS) second-order upwind scheme (least square cell based) for the spatial reconstruction of convective terms, while for the diffusive fluxes a cell-centred scheme is applied. An implicit scheme has been considered for time integration. Regarding air physical modelling, for present applications a perfect gas model has been employed (density by ideal gas law), the specific heat at constant pressure has been a polynomial function of temperature (from kinetic theory of gases), thermal conductivity has been derived by kinetic theory too, laminar viscosity has been calculated by classical Sutherland's law and turbulent viscosity has been computed by Spalart-Allmaras modelling. EFTV's surfaces have been assumed in radiative equilibrium, with wall emissivity $\varepsilon=0.4$ (asymptotic value for ZrO_2 coating), for all the flight conditions of Table 1 with the exception of $M_\infty=2$ flight condition for which adiabatic wall temperature has been assumed.

As far as boundary layer (BL) flow conditions are concerned, it is worth noting that a preliminary analysis based on criteria involving only free-stream conditions had indicated a transition altitude in the range of 35 km to 28 km.[14,15] However, the sensitivity of aerothermal loads to BL conditions and the large uncertainty on transition altitude, suggested to perform an analysis of laminar-to-turbulence natural transition along the reference design trajectory, (namely B-viscous), based on local flow conditions. Indeed, a number of viscous computations have been carried out with both laminar and turbulent BL assumptions for some flight conditions, thus allowing a more detailed (local) analysis based on both Di Cristina and Berry et al. criteria.[17,18] These two criteria allow detection of

natural laminar-to-turbulence transition for hypersonic waveriders. The first one, i.e. Di Cristina[17], which gives the local transition Reynolds number Re_{Xt} as a function of local edge Mach number M_e, reads:

$$\log_{10}(Re_{Xt}) = a \exp(b\, M_e^{\,c}) \qquad CRIT=\log_{10}(Re_X)/[a \exp(b\, M_e^{\,c})] \geq 1 \tag{2}$$

where a=6.421, b=1.209·10^{-4} and c=2.641. The effect of wing leading edge is also accounted for in the criterion by means of a function of wing sweep angle Λ, i.e.

$$(Re_{Xt})_\Lambda / (Re_{Xt})_{\Lambda=0} = 0.787 \cos^{4.346}\Lambda - 0.7221\, e^{-0.0891\Lambda} + 0.9464 \tag{3}$$

In the case of EFTV (Λ=80.1 deg) the "actual" Reynolds number is largely reduced, i.e. $(Re_{Xt})_\Lambda/(Re_{Xt})_{\Lambda=0}$=0.318, and this has a beneficial effect on the critical Reynolds number at which laminar-to-turbulence transition starts.

The second one, i.e. Berry et al.[17], was used in the frame of NASP project to study the X-43A boundary layer transition. It correlates the local transition Reynolds number based on momentum thickness Re_θ to the local edge Mach number M_e, i.e.

$$Re_\theta / M_e \geq 300 \div 450 \tag{4}$$

Figure 6 shows the planes (Y=0.0, 0.47 m) and sections (X=-0.2, 0.0, 0.5, 1.0, 1.5, 2.0, 2.5, 2.75 m) considered for the present analysis, and an application of the criterion used to detect BL edge from the (normal-to-wall) profiles of velocity and total enthalpy, i.e. H_{0e}=0.99·H_0.

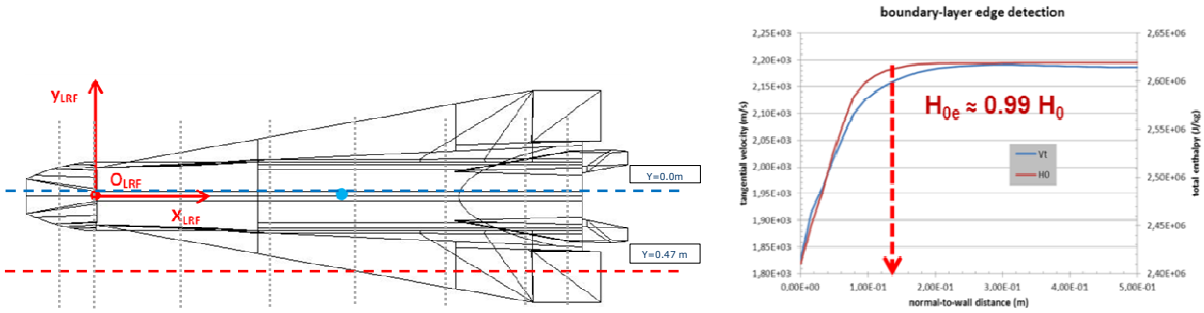

Figure 6. Planes and sections considered for the transition analysis (left) and BL profile with edge detection criterion (right).

After having extracted from laminar CFD solutions the BL profiles (in direction normal to the wall) of a number of flow properties (ρ, u, w, μ, T, Mach, H_0, δ, θ), the two criteria have been applied to the flight conditions along the reference trajectory corresponding to 37.71km, 33.06km and 29.93km. Results are reported in Figure 7 for the section Y=0.0m (fuselage) and Figure 8 for the section Y=0.47m (wing).

Note that for the calculation of Reynolds number X=0 has been assumed at nosetip (X=-0.4159 m in LRF) for the fuselage section, and at wing leading edge (X=1.72415 m in LRF) for the wing section.

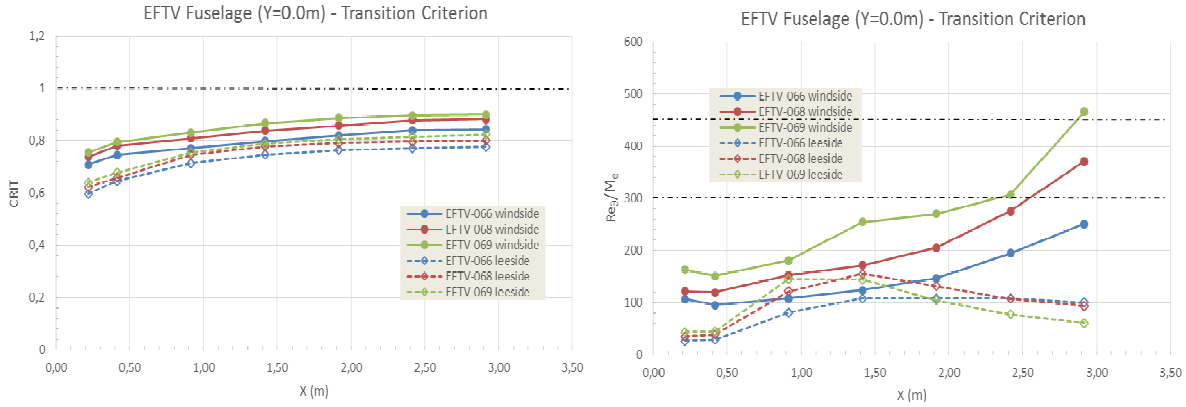

Figure 7. EFTV laminar-to-turbulence natural transition (fuselage): Di Cristina criterion (left) and X-43A criterion (right).

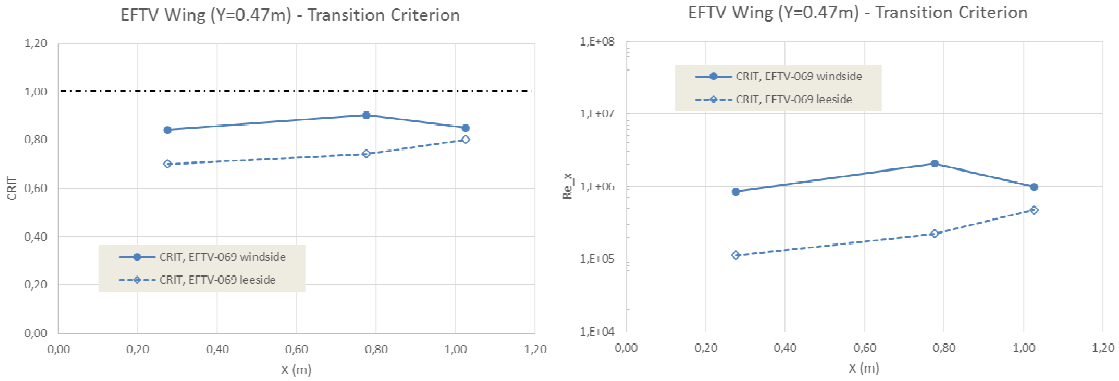

Figure 8. EFTV laminar-to-turbulence natural transition (wing): Di Cristina criterion (left) and local Reynolds number (right).

Regarding the fuselage, see Figure 7, a fully laminar flow is predicted on leeside by both criteria for the investigated conditions, while on windside laminar flow is predicted by Di Cristina's criterion whereas transition is predicted by the NASP criterion at the very rear of the fuselage: 2.55m from nosetip at 33.06km and 2.30m from nosetip at 29.93km. For what concerns the wing, the application of the Di Cristina criterion is displayed for the lower altitude case only, see Figure 8. Fully laminar flow both at leeside and windside is predicted (the effect of aileron's negative deflection is observed, too) due to the beneficial effect of wing sweep that strongly reduces local Reynolds number.

Considerations on step-induced laminar-to-turbulence transition (criterion based on k/δ, where k in the critical step height causing transition and δ the local BL thickness, Ref. 17) that could occur at the EFTV nose/fuselage junction on windside, and the identification of 29.93km altitude as sizing flight condition (combination of highest AoA and low altitude), have suggested that transition is triggered at altitude lower than 30 km with a step height of 1.2mm at the nose/fuselage interface. Therefore, considering also typical manufacturing and assembling admissible tolerances for such a junction, for the present CFD simulations flow is assumed fully laminar from EFTV-ESM separation to 33.06km altitude, and fully turbulent from 29.93km altitude to the end of mission.

A. CFD Results

Some CFD results of the flowfield past the EFTV glider are shown from Figure 9 to Figure 12. For instance, surface temperature contours on the full vehicle and an enlargement of the EFTV's forebody at 29.93km altitude and M_∞=7.25 (i.e. run-id EFTV-069) are provided in Figure 9. As shown, at these flight conditions the glider features local overheating at the nosetip, wing and fin leading edges as a result of nearly attached shock waves. Further, the upper panels of the fuselage and wings, and the portside of the right fin are due to the high angle of attack (α=12 deg); while the hotter leeside of the aileron is due to the negative flap deflection needed to trim the vehicle (δ_e=-

15.72 deg) at these Mach and attitude conditions. Three-dimensional flow streamtraces are provided along with the skin-friction lines on the glider's leeside (Figure 10). Vortices are observed on the leeside of the fuselage and wing with a large separated flow area due to the corner flow, whereas no significant flow separation is predicted at the hingeline for this maximum aileron deflection.

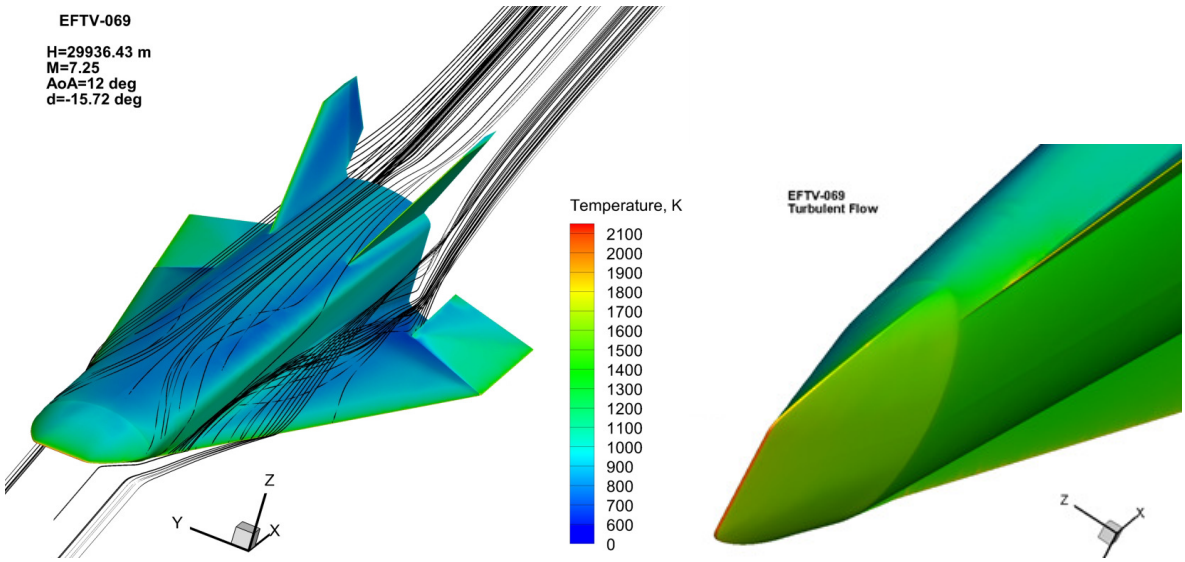

Figure 9. EFTV surface temperature contours (run-id EFTV-069) on full aeroshape (left) and forebody region (right).

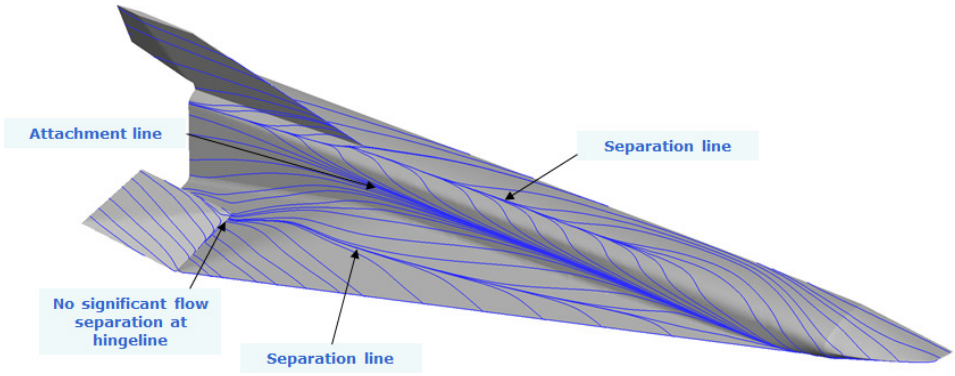

Figure 10. EFTV surface turbulent flow pattern (run-id EFTV-069).

EFTV's pressure distributions on the symmetry plane (section Y=0.0m) and mid-wing plane (section Y=0.47m) are reported in Figure 11 for a number of computed flight conditions from Table 1. For the condition EFTV-069 also the comparison between laminar and turbulent boundary layer is reported, showing no significant effect of turbulence on pressure for both leeside and windside. On the contrary, a strong effect of angle-of-attack and aileron's deflection has been predicted with varying flight conditions.

EFTV's convective heat flux (ε=0.4) distributions on the symmetry plane and mid-wing plane are shown in Figure 12 for the same flight conditions. The comparison between laminar and turbulent boundary layer results indicates no significant effect of turbulence on leeside, and a strong effect (roughly a factor two) of turbulence on windside, on the fuselage, the wing and aileron's leeside, too.

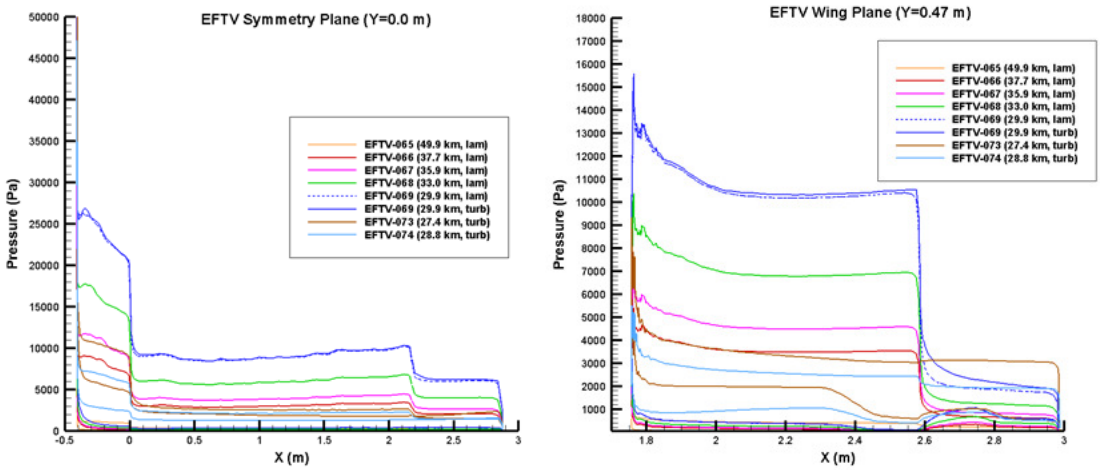

Figure 11. EFTV pressure distributions at Y=0.0m (left) and Y=0.47m (right) sections.

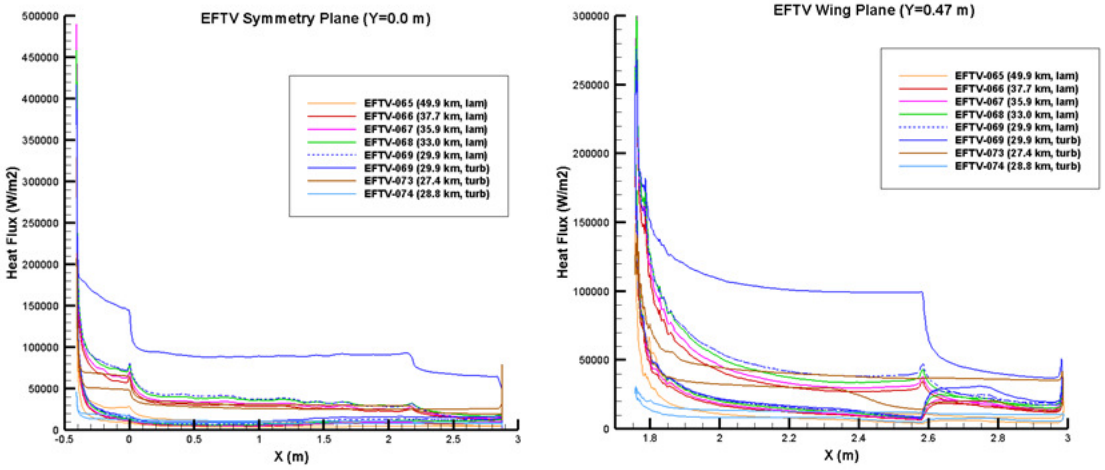

Figure 12. EFTV convective heat flux distributions at Y=0.0m (left) and Y=0.47m (right) sections.

As expected, the EFTV's forebody region has resulted critical from the thermal point of view. Indeed, the glider's aeroshape is very slender and with sharp leading edges both for fuselage nose and wing. Thus, focusing attention on forebody aeroheating a number of aeroshape cross-sections are considered, as shown Figure 13.

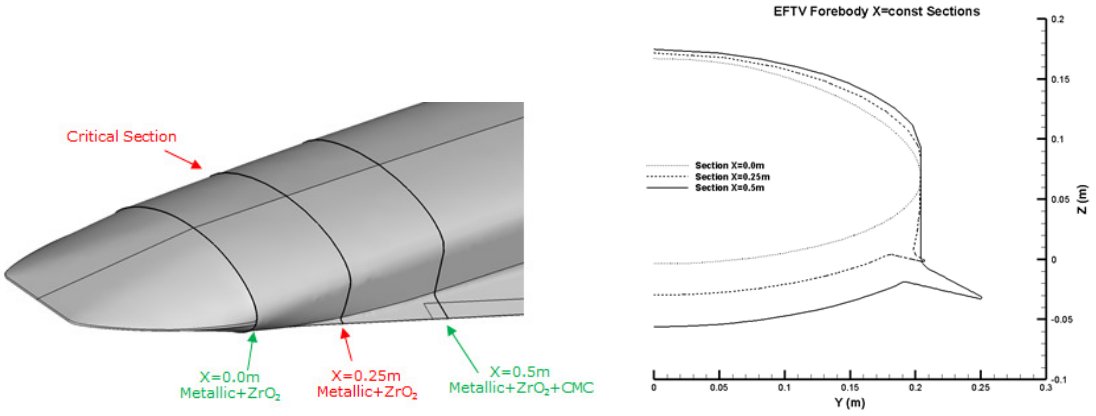

Figure 13. EFTV's forebody region and cross-sections for aeroheating analysis.

Results in terms of computed heat flux distributions on those sections and glider aeroshape are shown in Figure 14. As a result, the most critical section has resulted the one at X=0.25m, where the very small wing apex in titanium alloy plus coating is locally loaded by heat fluxes up to 250 kW/m^2.

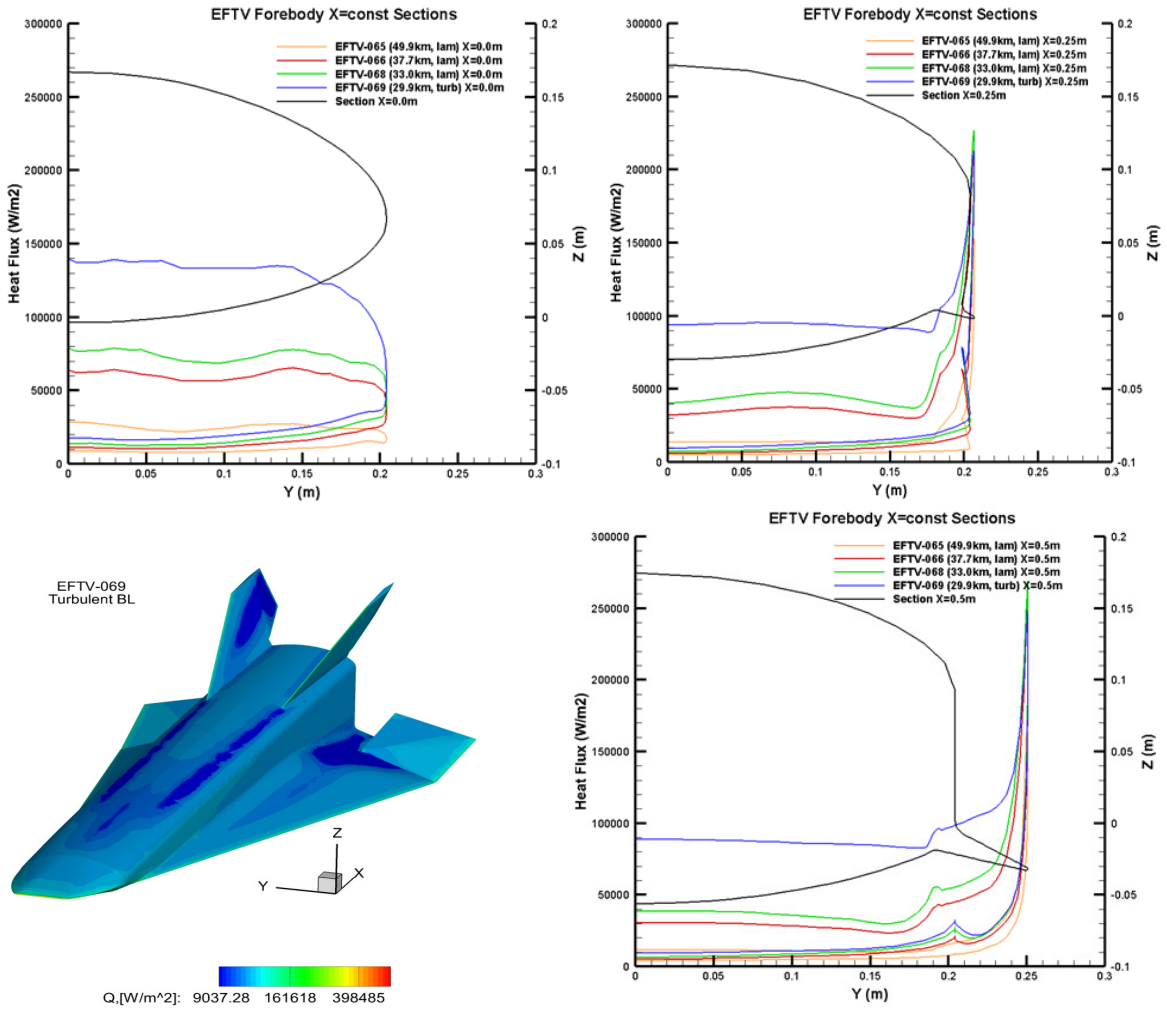

Figure 14. Heat flux distributions on EFTV's for several flight conditions.

IV. Thermal Design

A. Numerical Procedure

The vehicle thermal behaviour has been assessed by means of the FE method implemented in the software Ansys [19, 20]. A transient thermal analysis along the reference trajectory is performed to evaluate the time dependent temperature of the structure. The implemented numerical procedure is schematically reported in Figure 15.

In particular:

- The available CAD drawing of the vehicle is implemented in Ansys Workbench and properly modified, if required.
- The computational 3D mesh is generated.

- Steady CFD calculations (whose description is out of the scope of the present work) have been realized in a certain number of flight conditions to evaluate the convective heat transfer coefficient spatial distribution over the vehicle surface.
- The flight trajectory has been split in a certain number of legs, each of them characterized by a specific flight condition previously analysed by CFD (effect of angle of attack, aileron's deflection and Mach number are therefore considered, see Figure 16a).

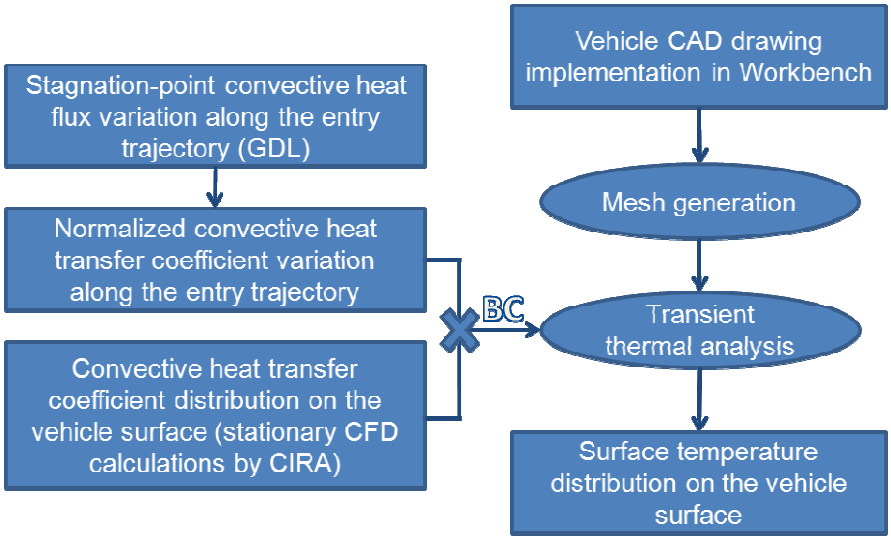

Figure 15. Numerical procedure flow chart

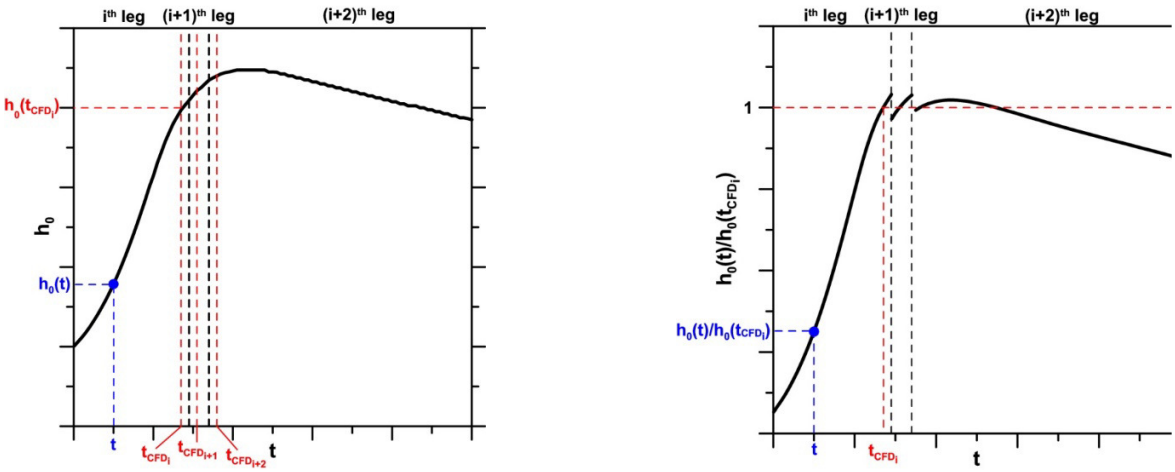

a) b)

Figure 16 a) Description of CFD results scaling along the trajectory. b) Typical normalized stagnation-point heat transfer function

- For each trajectory leg, the heat transfer coefficient distributions are properly scaled by the stagnation-point heat transfer coefficient variation along the selected trajectory leg, normalized with respect to the corresponding reference condition (i.e. the flight condition analysed by CFD). Referring to the nomenclature reported in Figure 16a, equation 5 is applied.

$$h(x,t) = h(x)|_{CFD_i} \cdot \frac{h_0(t)}{h_0(t_{CFD_i})} \quad (5)$$

An exemplary plot of the normalized stagnation-point heat transfer function, piecewise-defined in each trajectory leg, is shown in Figure 16b. In particular, the stagnation-point convective heat transfer coefficient has been estimated scaling the cold wall stagnation-point convective heat flux variation along the trajectory by the stagnation temperature profile, as reported in equation (6).

$$h_0 = \frac{\dot{q}_{0,cw}}{T_0} \quad (6)$$

In turn, the cold wall stagnation-point convective heat flux variation along the trajectory has been evaluated according to the Tauber's model. [21]

- The transient thermal analysis is then set assuming, as convective boundary condition, the heat transfer coefficient evaluated according to the previously discussed procedure and the stagnation temperature profile (in coherence with the CFD modelling). A radiative dissipation condition is also considered for all the external surfaces. Therefore the overall condition reported in equation (7) is applied.

$$\dot{q} = h \cdot (T_0 - T_w) - \sigma \cdot \varepsilon \cdot T_w^4 \quad (7)$$

B. Candidate Materials

Different classes of materials have been preliminarily selected and analysed for the EFTV and the ESM structures, namely: titanium alloy, aluminium, copper, C/C-SiC and zirconia (ZrO_2) for surface coatings. This should give a first estimation of the characteristic behaviour of potential materials along the analysed flight trajectory.

Titanium alloys exhibit a unique combination of mechanical and physical properties and corrosion resistance which have made them desirable for critical, demanding aerospace applications, also in high temperatures conditions. Aluminium is widely used in the aerospace field for its excellent strength to weight ratio. Copper is employed in this case as a heat sink to accommodate the thermal energy in some critical components (e.g. nose, leading edges). C/C-SiC developed at DLR[22] and tested in different high temperatures applications (e.g. HIFiRE and SHEFEX) is considered for ailerons and for the final part of the wing leading edge. A zirconia (ZrO_2) coating layer has been also considered to protect metallic components, increasing their surface emissivity and confining the larger temperatures on the coating itself.

Thermal and mechanical properties of titanium alloy and zirconia coating have been provided by TsAGI, Tsentralniy Aerogidrodinamicheskiy Institut (Central Aerohydrodynamic Institute), which is in charge of the system manufacturing.

Table 2 reports the materials selected for the EFTV components highlighted in Figure 17. In particular:

- copper for the vehicle nose;
- copper for the fore part of the wing leading edges;
- C/C-SiC for the remaining part of the wing leading edge;
- copper for the leading edge of the V-tails;
- C/C-SiC for the ailerons;
- titanium alloy for the remaining parts of the structure.

EFTV					
Nose	**Fuselage**	**Wing**	**Wing LE**	**V-Tail**	**Aileron**
Copper	Ti-Alloy	Ti-Alloy	C/C-SiC / Copper Ti (linked to frame 1)	Ti-Alloy / Copper	C/C-SiC

Table 2. Preliminarily material selection for the main EFTV structural components.

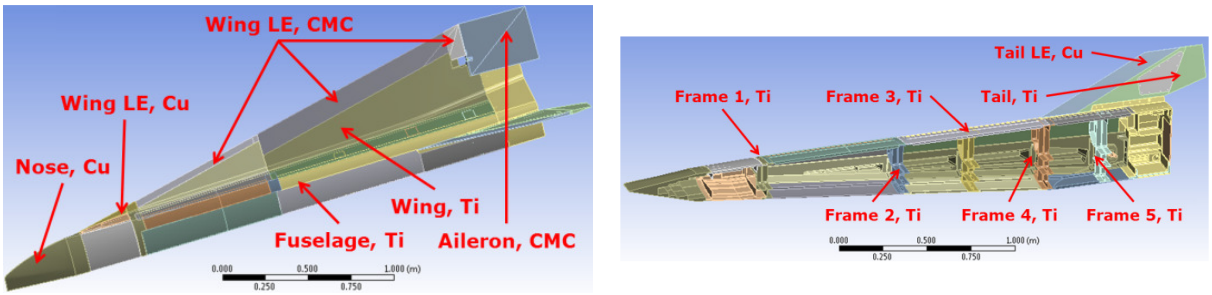

Figure 17. Main structural components of the analysed EFTV

C. Preliminary results

As results, according to the previously discussed method, the temporal variation of the maximum temperature on the different analysed materials and vehicle components has been plotted along the flight path.

Thermal Analysis starts from point 1 to the end of mission in Figure 18, where points representing time instants used to rebuild the trajectory are:

1. fairing ejection at about 82 Km;
2. payload release at apogee (90 Km);
3. ESM separation at about 50 Km;
4. 6 CFD points: EFTV-065, EFTV-066, EFTV-067, EFTV-068, EFTV-069, EFTV-073 (see Table 1).

Initial temperature condition considered for the whole EFTV's structure is 27°C as indicated by DLR-Moraba as the most suitable temperature at fairing opening. Sizing heat fluxes based on hypothesis of laminar-to-turbulence transition at 30 km altitude (EFTV-069) have been considered. Uncertainties are also included in margins definition. In particular following hypothesis have been taken into account:

- Laminar flow: 20% (Reynolds effect due to 1 km trajectory dispersion, CFD code-to-code error)
- Turbulent flow: 35% (Reynolds effect due to 1 km trajectory dispersion, CFD code-to-code error, turbulent modelling error)

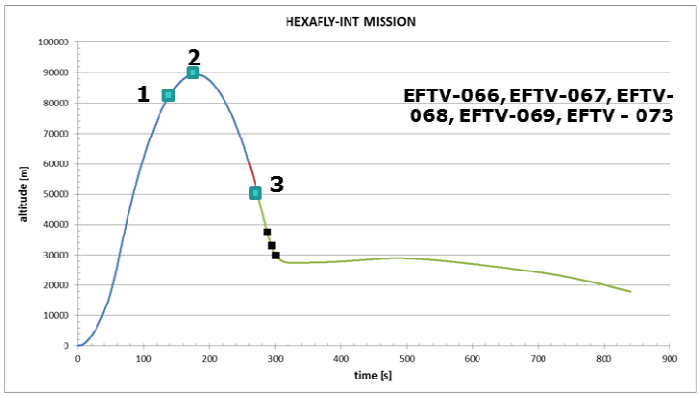

Figure 18. Thermal analysis mission profile used

Two different FEM models (Figure 19 and Figure 20) have been considered on a half-sized vehicle in this preliminary phase:

- Model 1 (FEM 1): 3D mesh with 1 mm zirconia coating leeside and windside (580k nodes)
- Model 2 (FEM 2): 3D mesh with 1 mm ZrO2 coating only nose and windside (not on leeside) (400k nodes)

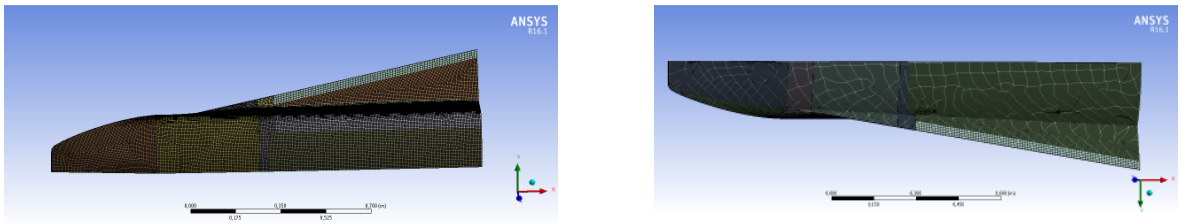

Figure 19. Finite Element Model 1

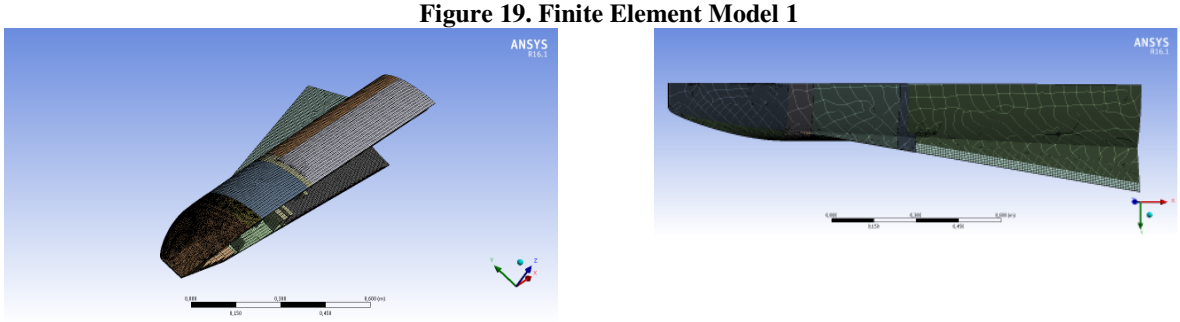

Figure 20. Finite Element Model 2

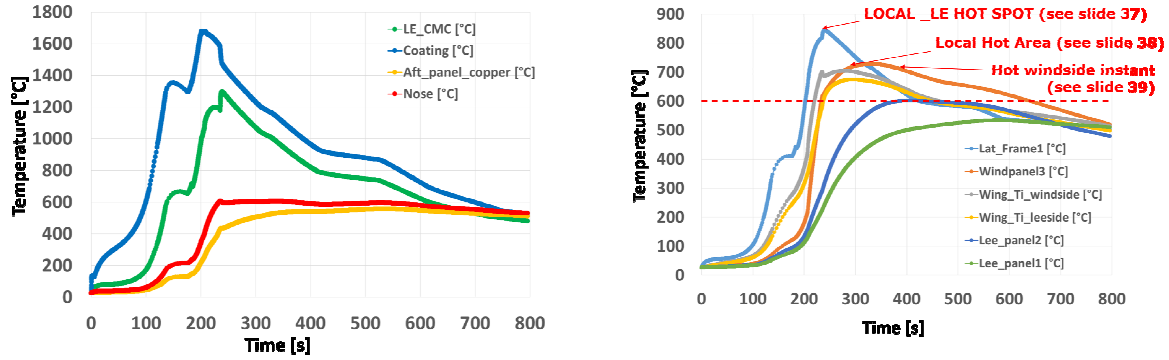

(a) Cu, CMC, ZrO2 (b) Ti

Figure 21. Maximum temperature along the flight profile on the main components (FEM 1)

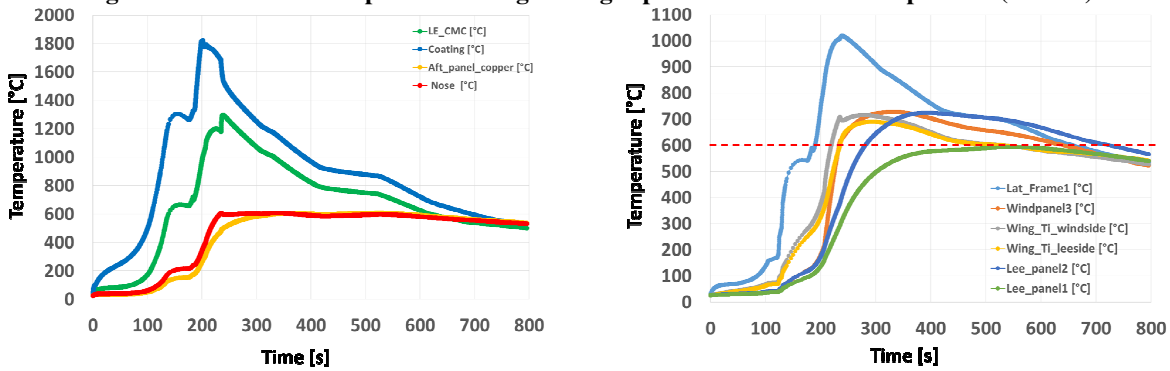

(a) Cu, CMC, ZrO2 (b) Ti

Figure 22. Maximum temperature along the flight profile on the main components (FEM 2)

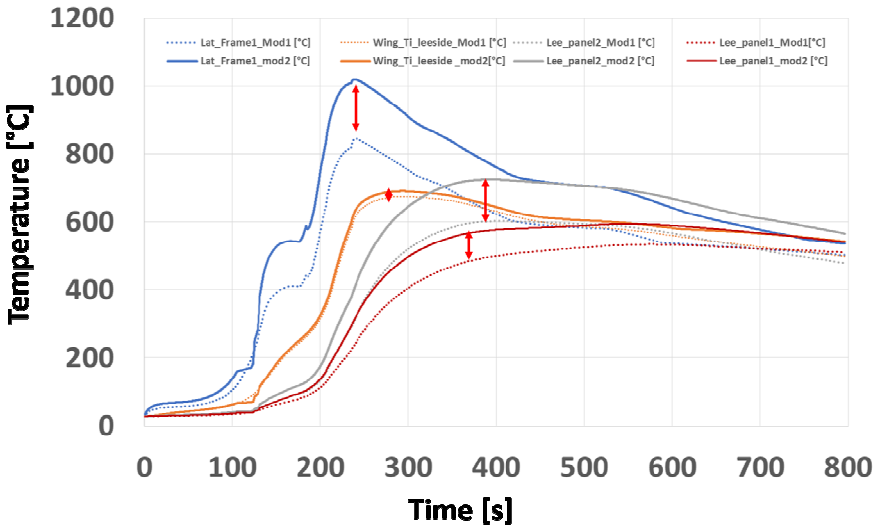

Figure 23. Comparison FEM 1 and FEM 2. Evaluation of coating effect on Ti

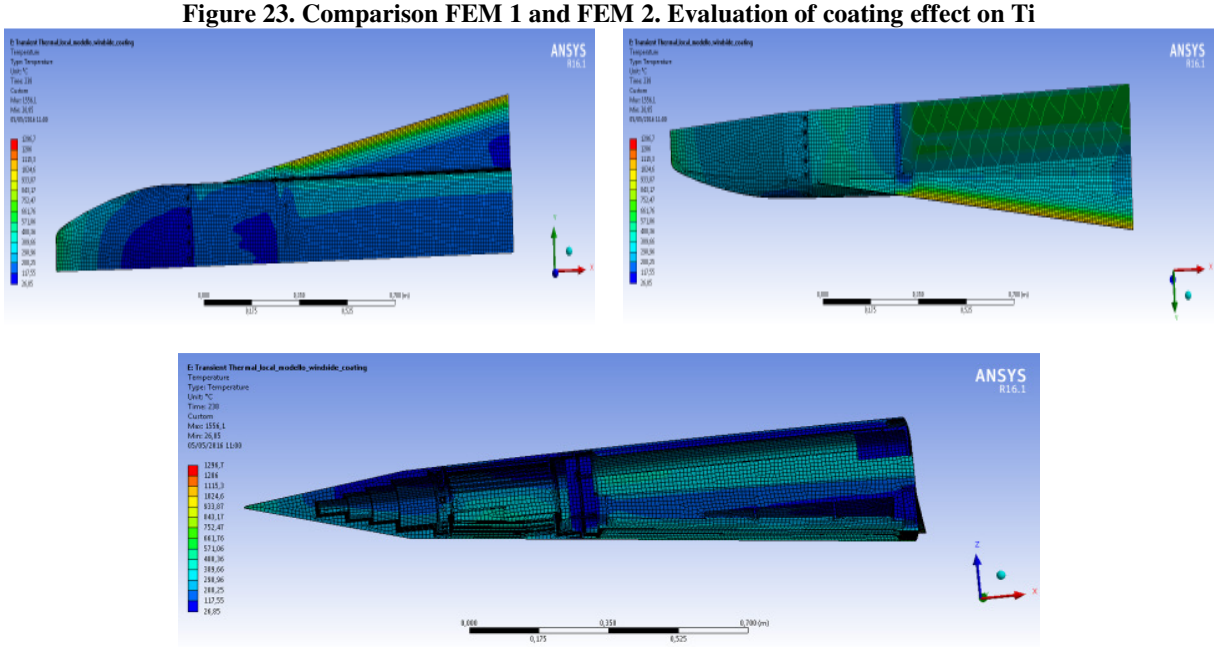

Figure 24. Temperature distribution, at the peak heating condition for structural components of the EFTV

	Lat Frame 1	Wing lee	Lee panel 2	Lee panel 1
FEM 1	840	660	600	500
FEM 2	1020	695	740	600

Table 3. Comparison FEM 1 and FEM 2. Maximum temperature on Titanium components.

From Figure 21 and Figure 22 it can be seen that zirconia coatings, C/C-SiC and copper components on EFTV (having maximum service temperatures, respectively, in the order of 2400°C, 1600°C and 800°C) would widely survive the aerothermal environment in these conditions. On the other hand, it can be noted that the maximum temperatures on the titanium structures slightly exceed their upper working temperature limits (600 °C). This is attenuated by coating the leeside as shown in Figure 23 except for a titanium leading edge linked to the frame 1 (see results in Table 3). Figure 24 shows the temperature distribution, at the peak heating condition, for structural

components of the EFTV. This means that such temperature overshoot can be in principle redistributed inside the vehicle structure through a future thermal structural optimization.

V. Conclusions

Aero-thermal simulations presented in the paper are not definitive. Indeed, they have been performed on a sizing reference trajectory that is not the final one and assuming a vehicle mass of 350kg. Anyway, it has been already assessed that the final vehicle and trajectory will not change significantly from now on. Therefore, it can be finally concluded that a thermal model has been realized for the EFTV structure on the basis of aero-thermal loads estimated along the flight path. Zirconia coating guarantees a relatively large surface emissivity and a suitable thermal protection for the underlying materials. Copper seems to be adequate for the EFTV nose and the first part of the wing leading edge, considering its ability to work as a heat sink. Copper structures and titanium structures on EFTV can withstand the aerothermal environment except for limited spots, requiring a proper thermal structural optimization. Thermal-structural design is still ongoing and a numerical analysis campaign will be performed on the basis of an updated structural configuration, flight trajectory and aerothermal environment.

Acknowledgments

This work was performed within the 'High-Speed Experimental Fly Vehicles-International' project fostering International Cooperation on Civil High-Speed Air Transport Research. HEXAFLY-INT, coordinated by ESA-ESTEC, is supported by the EU within the 7th Framework Programme Theme 7 Transport, Contract no.: ACP0-GA-2014-620327 and by the Ministry of Industry and Trade, Russian Federation. Further info on HEXAFLY-INT can be found on http://www.esa.int/hexafly-int.

References

1. Steelant J., "Achievements obtained on Aero-Thermal Loaded Materials for High-Speed Atmospheric Vehicles within ATLLAS," 16th AIAA/DLR/DGLR International Space Planes and Hypersonic Systems and Technologies Conference, AIAA-2009-7225, Bremen, Germany, 2009.
2. Steelant, J., "Sustained Hypersonic Flight in Europe: first achievements within LAPCAT II," 17th AIAA International Space Planes and Hypersonic Systems and technologies conference, AIAA 2011-2243, San Francisco, CA, 2011.
3. Steelant, J., Langener, T., Hannemann, K., Marini, M., Serre, L., Bouchez, M., Falempin, F., "Conceptual Design of the High-Speed Propelled Experimental Flight Test Vehicle HEXAFLY," 20th AIAA International Space Planes and Hypersonic Systems and technologies conference, AIAA 2015-3539, Glasgow, Scotland, 2015.
4. Carandente, V., Scigliano R., "Thermo-Structural Design of the Hexafly-INT Experimental Flight Test Vehicle (EFTV) and Experimental Service Module (ESM)," *57thAIAA/ASCE/AHS/ASC Structures, Structural Dynamics, and Materials Conference,* AIAA 2016-1716, San Diego, California, USA, 2016.
5. Scigliano R., Carandente V., Favaloro N., Cardone S., Steelant J., "Thermo-Structural Design of The Hexafly-Int Experimental Flight Test Vehicle,"*, Proceedings of the ASME 2015 International Mechanical Engineering Congress and Exposition*, IMECE2015-50930, Houston, Texas, USA, 2015.
6. Scigliano R., Carandente V., " Design Analysis of the Hexafly-int Thermal Protection System", 8th European Workshop on TPS & Hot Structures, 19-22 April 2016, ESA/ESTEC, Noordwijk, The Netherlands.
7. Pezzella, G., Marini, M., Reimann, B., Steelant, J., "Aerodynamic Design Analysis of the Hexafly-INT Hypersonic Glider", 20th AIAA International Space Planes and Hypersonic Systems and Technologies Conference, Glasgow, Scotland, 6-9 July 2015: AIAA-2015-3644.
8. Prabhu, D. K., "System Design Consraints – Trajectory Aerothermal Environments". Paper presented at the RTO AVT Lecture Series on "Critical Technologies for Hypersonic Vehicle Development", held at the von Kármán Institute, Rhode-St-Genèse, Belgium, 10-14 May, 2004, and published in RTO-EN-AVT-116.
9. Steelant, J., Varvill, R., Defoort, S., Hannemann, K., and Marini, M., "Achievements Obtained for Sustained Hypersonic Flight within the LAPCAT-II project", 20th AIAA International Space Planes and Hypersonic Systems and Technologies Conference, Glasgow, Scotland, July 6-9, 2015: AIAA-2015-3677.
10. Meerts, C., Steelant, J., "Air Intake Design for the Acceleration Propulsion Unit of the LAPCAT-MR2 Hypersonic Aircraft", in 5th European Conference for Aeronautics and Space Sciences (EUCASS), Munich, July 1-5, 2013.
11. Pezzella, G., Marini, M., Cicala, M., Vitale, A., Langener, T., Steelant, J., "Aerodynamic Characterization of HEXAFLY Scramjet Propelled Hypersonic Vehicle", 32nd AIAA Aviation (Applied Aerodynamics Conference), 16-20 June 2014, Atlanta, GA: AIAA 2014-2844.

12. Steelant, J., Langener, T., Di Matteo, F., Hannemann, K., Riehmer, J., Kuhn, M., Dittert, C., Scheuerpflug, F., Jung, W., Marini, M., Pezzella, G., Cicala, M., Serre, L., "Conceptual Design of the High-Speed Propelled Experimental Flight Test Vehicle HEXAFLY", 20th AIAA International Space Planes and Hypersonic Systems and Technologies Conference, Glasgow, Scotland, 6-9 July 2015: AIAA-2015-3539.
13. Favaloro, N., Pezzella, G., Carandente, V., Scigliano, R., Cicala, M., Morani, G., Steelant, J., "Design Analysis of the High-Speed Experimental Flight Test Vehicle HEXAFLY-International". 20th AIAA Hypersonics. Strathclyde University Technology & Innovation Center. 6-9 July 2015 Glasgow. Scotland. AIAA-2015-3607. doi: 10.2514/6.2015-3644.
14. Pezzella, G., Carandente, V., Scigliano, R., Marini, M., Steelant, J., "Aerothermal Environment Methodology of the Hexafly-Int Experimental Flight Test Vehicle (EFTV)", 8th European Symposium on Aerothermodynamics for Space Vehicles. 2-6 March 2015. Lisbon. Portugal. European Space Agency.
15. Carandente, V., Scigliano, R., Pezzella, G., Marini, M., and Steelant, J., "Finite Element Thermal Design of the Hexafly-INT Experimental Flight Test Vehicle". 6th European Conference for Aeronautics and Space Sciences (Eucass). 29 June- 3 July. 2015 Krakow. Poland.
16. Di Benedetto, S., Di Donato, M.P., Rispoli, A., Cardone, S., Riehmer, J., Steelant, J., Vecchione, L., "HEXAFLY-INT Project: Design of a High Speed Flight Experiment", Hypersonic from 100.000 to 400.000 ft, 2nd International Symposium on Hypersonic Flight, Rome, Italy, 30 June-1 July, 2016.
17. Di Cristina, V., "Three-Dimensional Laminar Boundary-Layer Transition on a Sharp 8-deg Cone at Mach 10", AIAA Journal, Vol. 8, No. 5, May 1970, p. 855.
18. Berry, S., et al., "Boundary Layer Transition on X-43A", 38th AIAA Fluid Dynamics Conference, Seattle WA, USA, 23-26 June 2008: AIAA-2008-3736.
19. ANSYS Inc., Thermal analysis guide, Release 16.1, 2015.
20. ANSYS Inc., Structural analysis guide, Release 16.1, 2015.
21. Tauber, M. E., "A review of high-speed, convective, heat-transfer computation methods," NASA Technical Paper 2914, 1989.
22. Glass, D. E., Capriotti, D. P., Reimer, T., Kütemeyer, M., Smart, M., "Testing of DLR C/C-SiC and C/C for HIFiRE 8 Scramjet Combustor," *19th AIAA International Space Planes and Hypersonic Systems and Technologies Conference*, Atlanta, Georgia, USA, 2014.